Production of dense, cool plasmas by multiphoton ionization of sodium vapor

O. L. Landen* and R. J. Winfield†
Blackett Laboratory, Imperial College, London SW7 2BZ, United Kingdom
(Received 24 August 1984; revised manuscript received 25 June 1985)

Cool, dense plasmas were produced by two-photon resonant ($3s \rightarrow 3d$) three-photon ionization of sodium vapor by a 0.5-MW pulsed dye laser operating at $\lambda = 6854$ Å. Electron densities were deduced from the width and shift of the $3p$-$4d$ line shape observed in emission and from the intensity of the dipole-forbidden component $3p$-$4f$. Electron temperatures were calculated from ratios of line intensities by assuming partial local thermodynamic equilibrium. A minimum of 1 electron per Debye sphere was achieved and the degree of nonideality shown to be limited by collisional recombination.

I. INTRODUCTION

Laser-induced multiphoton ionization of sodium atoms has recently been studied both theoretically[1–5] and experimentally[6,7] with particular emphasis on ionization enhancement when tuning close to a one- or two-photon atomic resonance. The electron density yield has been shown to be a sensitive function of laser wavelength for near-resonant conditions. The electron temperature, in the absence of collisional recombination and inverse bremsstrahlung heating, should just be a function of photon energy and ionization potential. Hence, a suitable laser wavelength can be found for which the electron density N_e is maximized, the electron temperature T_e is minimized, and thus a nonideal plasma is approached.

Plasmas with a minimum of 1 electron per Debye sphere produced by resonant pumping of sodium vapor and diagnosed by emission spectroscopy are described in the preceding paper, hence referred to as I.[8] The aims of the present experiment were to confirm the results of I and investigate the degree of nonideality achievable by laser photoionization.

II. IONIZATION SCHEME

The resonantly enhanced single-wavelength photoionization scheme yielding the minimum photoelectron energy in sodium is the two-photon-resonant ($3s \rightarrow 3d$) three-photon ionization process at $\lambda = 6854$ Å. The scheme is shown in Fig. 1, producing a photoelectron temperature of 0.19 eV. The two-photon transition cross section for $3s \rightarrow 3d$ has been calculated and verified experimentally for a 140-mÅ bandwidth laser as $\sigma_2 = 10^{-42}$ cm^2 s.[9] The single-photon ionization cross section from the $3d$ state for $\lambda = 6584$ Å is $\sigma_1 = 1.5 \times 10^{-17}$ cm^2.[10] Ignoring stimulated and spontaneous radiative decay from the $3d$ state and electron recombination and deexcitation, the relevant rate equations are

$$\frac{dN(3d)}{dt} = N(3s)\sigma_2 F^2 - N(3d)\sigma_1 F \,, \tag{1}$$

$$\frac{dN_e}{dt} = N(3d)\sigma_1 F \,, \tag{2}$$

where F, the photon flux in photons cm^{-2} s^{-1}, is related to the laser flux I by $F = 3.5 \times 10^{18} I/\mathrm{W\,cm^{-2}}$. Integrating Eq. (1) for $N(3s)$ approximately constant, substituting for $N(3d)$ in Eq. (2), and integrating Eq. (2) yields

$$N_e = N(3s)\sigma_2 F^2 \left[t - \frac{1}{\sigma_1 F}(1 - e^{-\sigma_1 F t}) \right] . \tag{3}$$

After substituting for cross sections,

$$\frac{N_e}{N(3s)} = 10^{-5} I^2 \left[t - \frac{1}{50I}(1 - e^{-50It}) \right] . \tag{4}$$

For small I such that $50It \ll 1$, Eq. (4) reduces to $N_e/N(3s) \propto I^3$ which corresponds to single-step multiphoton ionization and an unsaturated $3d$ level. By Eq. (4), 50% ionization should occur within 10 ns for a modest laser flux $I = 3$ MW cm^{-2}.

III. EXPERIMENTAL DETAILS

The experimental setup was similar to that described in I with three modifications. The dye laser pumped by a 300-mJ, 30-ns frequency-doubled Nd:glass laser consisted

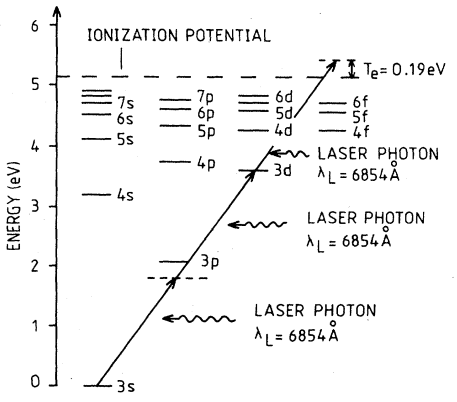

FIG. 1. Sodium-term diagram depicting multiphoton ionization scheme.

of only two dye amplifier cells. The laser output at 6854 Å was maximized to 10 mJ in 22 ns by using a dye solution of 4 parts to 1 part rhodamine-B—Oxazine 725 in methanol. The laser beam was focused to 0.3 mm^2 at the center of a sodium oven. Emission line shapes were viewed at 90° to the laser beam as in I with 15 ns, 2 Å resolution using a 30-cm grating Bentham spectrometer, RCA 7265 photomultiplier, and Tektronix 466 storage oscilloscope. Line shapes were recorded on a shot-to-shot basis.

IV. RESULTS OF EMISSION SPECTROSCOPY

The laser-excited sodium vapor exhibited a white glow and all atomic doublet transitions $3p$-nd for $3 \leq n < 9$ and $3p$-ns for $5 < n < 9$ were observed. The fluorescence and electron density yields were optimized by laser tuning in 0.1-Å steps. Emission line shapes were obtained for the strongest and most useful transitions for diagnosing the electron density, $3p$-$3d$ and $3p$-$4d$, at sodium densities $N_{Na} = 2\times10^{16}$, 5×10^{16}, 7×10^{16}, 10^{17}, and 2×10^{17} cm^{-3} and also for $3p$-$5s$ at 10^{17} cm^{-3}. Line shapes were recorded between 50 and 400 ns after the start of the plasma. A low-pressure Phillips sodium lamp was used for wavelength calibration. Two of the line shapes are presented in Figs. 2 and 3 for $N_{Na} = 10^{17}$ cm^{-3}. The intensity ratios for the peaks of the doublets clearly shows that $3p$-$3d$ and $3p$-$4d$ are optically thick and thin, respectively. In addition, the $3p$-$4d$ line shape shows plasma-induced broadening, shift, and the emergence of the dipole-forbidden components $3p$-$4f$ due to the plasma microfield. Line shapes recorded during laser irradiation ($t < 50$ ns) had an additional spike at line center of similar duration to the laser pulse, 20 ns. The spike is tentatively attributed to stimulated emission from transient population inversions between high-lying levels and the $3p$ state created by (a) laser pumping of the $3d$ level, (b) preferential electron recombination into high-lying levels at a rate approximately proportional to n^{6}.[11]

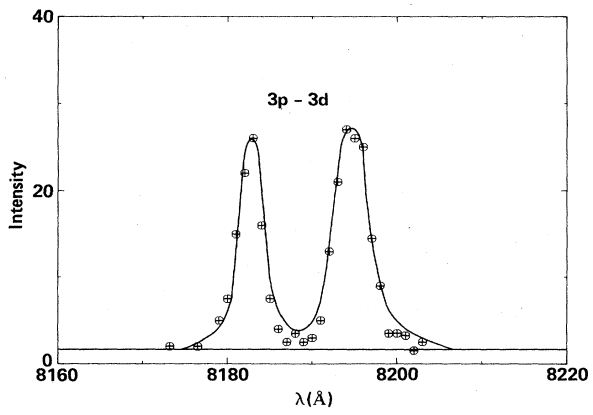

FIG. 2. $3p$-$3d$ emission line shape for $N_{Na} = 10^{17}$ cm^{-3}, $t = 100$ ns. Solid line is continuum level and solid curve is theoretical fit (Ref. 15) including radiation transport.

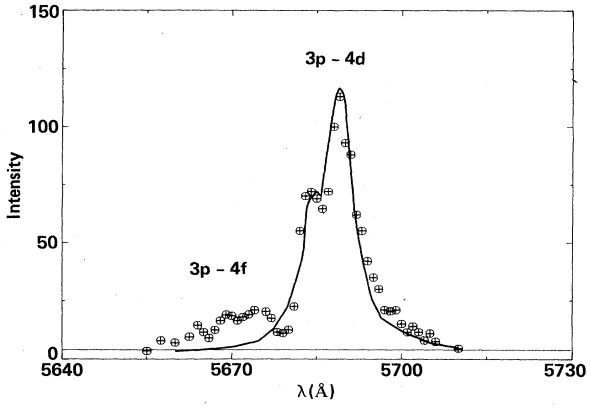

FIG. 3. $3p$-$4d$ emission line shape for $N_{Na} = 10^{17}$ cm^{-3}, $t = 200$ ns. Solid line is continuum level and solid curve is theoretical fit (Ref. 15) excluding forbidden components and including radiation transport.

V. ANALYSIS OF EMISSION SPECTROSCOPY

A. Electron density

1. Linewidths

The four dominant sources of line broadening were determined in I to be instrumental, resonance, opacity, and plasma induced. The Gaussian instrument profile of full width at half maximum 1.8—2.3 Å was first deconvolved from the experimental line shapes. Since no self-absorption was observed, the combined effects of opacity and plasma perturbation can be calculated by considering radiation transport through a homogeneous slab of width X:

$$I(\lambda-\lambda_0) = B(T)\left[1-\exp\left[-\frac{\lambda_0^2 e^2 f X N(3p)\Delta\lambda}{4\pi\epsilon_0 mc^2[(\lambda-\lambda_0)^2+\Delta\lambda^2]}\right]\right],$$

where $B(T)$ is the blackbody flux, λ_0 is the line-center wavelength, f is the transition oscillator strength,[12,13] and $\Delta\lambda$ is the sum of the resonance width[14] and plasma-induced width.[15] The two variables, N_e and $N(3p)$, can be deduced as in I by comparing linewidths from at least two transitions.[16] The temporal history of N_e for $N_{Na} = 5\times10^{16}$ and 10^{17} cm^{-3} is shown in Fig. 4. A peak $N_e = (2.1\pm0.5)\times10^{16}$ cm^{-3} was recorded for $N_{Na} = 2\times10^{17}$ cm^{-3}, equivalent to the highest N_e registered for resonant pumping in I.

2. Stark shifts

The ratio of shift to width of the $3p_{3/2}$-$4d_{5/2}$ transition versus electron density determined by the width is plotted in Fig. 5. The solid and dashed line represent calculated ratios with and without Debye shielding, respectively. As in I, better agreement is found by including Debye screening.

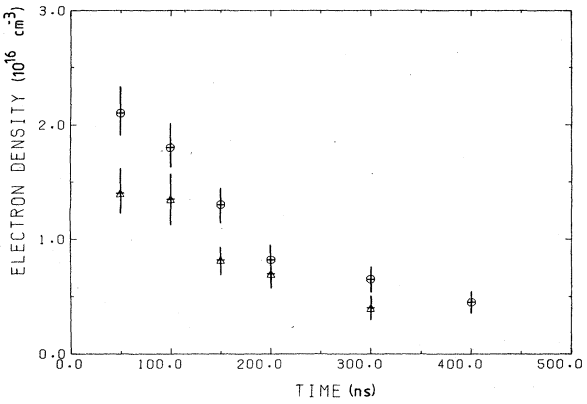

FIG. 4. Temporal history of N_e deduced from $3p$-$4d$ linewidths. (⏃) $N_{Na}=5\times10^{16}$ cm^{-3}; (⊕) $N_{Na}=10^{17}$ cm^{-3}.

3. *Forbidden components*

The spectrally integrated ratio of $3p$-$4f$ forbidden-component intensity to $3p$-$4d$ allowed-transition intensity is also an electron density diagnostic. The ratio of electron densities determined by such forbidden-component intensities and by the $3p$-$4d$ width is shown in Fig. 6 versus electron density determined from the $3p$-$4d$ width. Agreement is good at low densities ($N_e<1.5\times10^{16}$ cm^{-3}). The discrepancy at higher densities is probably due to the breakdown of the perturbation theory used since the intensity ratio of forbidden component to allowed transition has reached 20% at $N_e=1.5\times10^{16}$ cm^{-3}.

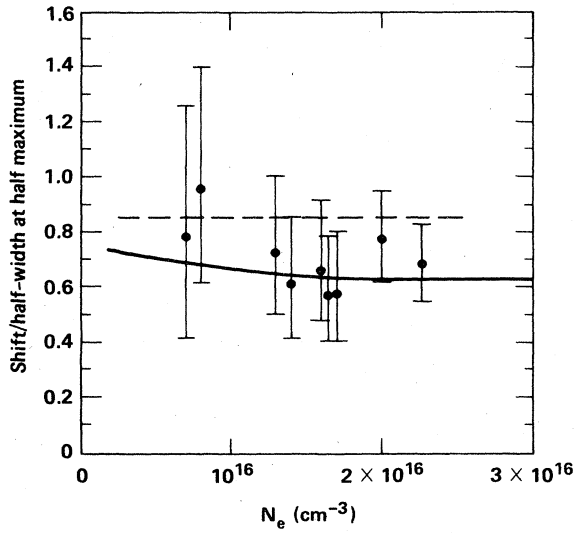

FIG. 5. $3p$-$4d$ shift-to-width ratio vs N_e measured from $3p$-$4d$ widths. Dashed line represents theory without shielding and solid line includes Debye shielding.

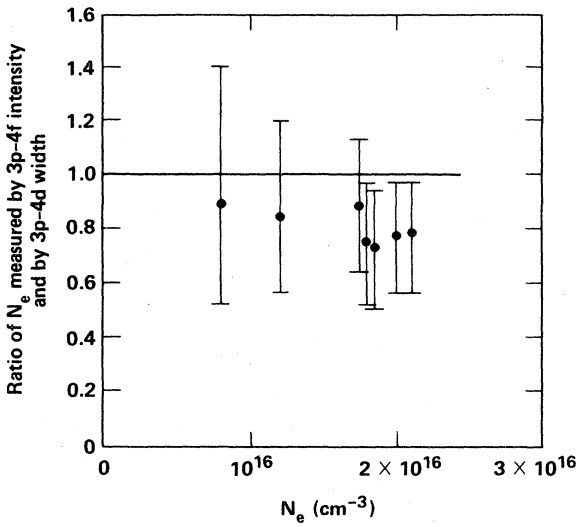

FIG. 6. Ratio of N_e measured by intensity of $3p$-$4f$ forbidden component and by $3p$-$4d$ width vs N_e measured from $3p$-$4d$ width. Solid line represents same N_e measured by both diagnostics.

B. Electron temperature

The electron temperatures were deduced as in I from ratios of line intensities after correcting for radiation reabsorption by dimers[17] and atoms and accounting for the spectral sensitivity of the detection system. A typical Boltzmann plot for $N_{Na}=2\times10^{16}$ cm^{-3}, $t=100$ and 400 ns is shown in Fig. 7. All levels above $3d$ appear to be in local thermodynamic equilibrium, as predicted in I. The temporal history of T_e is shown in Fig. 8 for $N_{Na}=2\times10^{16}$ and 5×10^{16} cm^{-3}. Four possible reasons why T_e exceeded the photoionization temperature 0.19 eV include ionization potential depression,[18] inverse bremsstrahlung heating, heating by three-body collisional recombination, and superelastic collisions depopulating the $3d$ level. Only three-body recombination can explain

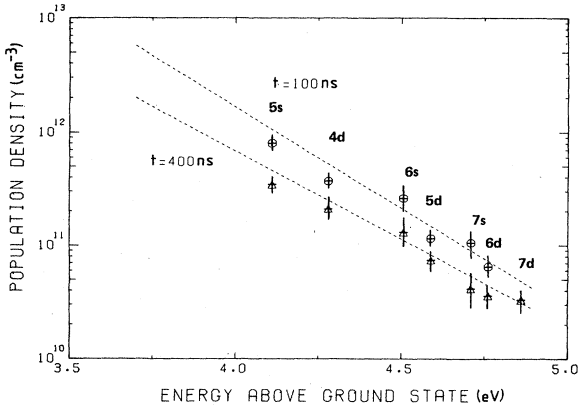

FIG. 7. Boltzmann plot for $N_{Na}=2\times10^{16}$ cm^{-3}. (⏃) $t=100$ ns; (⊕) $t=400$ ns.

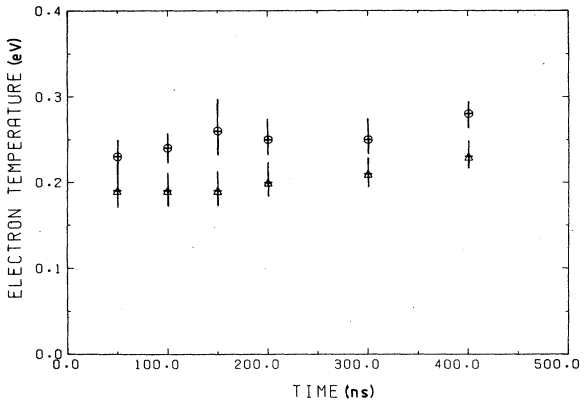

FIG. 8. Temporal history of T_e. ($\triangle$) $N_{Na}=2\times10^{16}$ cm^{-3}; ($\oplus$) $N_{Na}=5\times10^{16}$ cm^{-3}.

the gradual rise in T_e after the end of the laser pulse. The inverse bremsstrahlung heating rate during the laser pulse is given by[19]

$$\frac{dT_e}{dt}=\frac{10^{-18}\lambda_L^2 N_e I g}{T_e^{3/2}}\ , \tag{5}$$

where λ_L is the laser wavelength in μm and g, the free-free Gaunt factor, is between 1 and 1.5 for $T_e<1$ eV, $\lambda<1$ μm.[20] Electron-atom inverse bremsstrahlung can be neglected for $>1\%$ fractional ionization.[21] For $\lambda=6854$ Å, $N_e=2\times10^{16}$ cm^{-3}, $T_e=0.2$ eV, and $I\approx10^8$ W cm^{-2}, the initial heating rate by Eq. (5) is

$$\frac{dT_e}{dt}=0.01\text{ eV ns}^{-1}\ . \tag{6}$$

In fact, the temperature increase will be smaller as observed experimentally since a large fraction of the energy gained by the free electrons is used for subsequent collisional excitation and ionization,[22] and thermalization of atoms and ions.[23]

C. Plasma recombination

The temporal history of the electron density during laser irradiation can be represented by a rate equation including multiphoton ionization and three-body recombination. Diffusion described in I can be ignored at early times ($t<50$ ns). Hence,

$$\frac{dN_e}{dt}=(N_{Na}-N_e)\sigma F^n-\alpha(T_e)N_e^3\ . \tag{7}$$

σF^n is the ionization rate and $\alpha(T_e)$ is a three-body recombination coefficient. The two limits of Eq. (7) are as follows.

(a) The recombination rate is negligible compared to the ionization rate even by the end of the laser pulse. Hence,

$$N_e/(N_{Na}-N_e)=\text{const}\ .$$

(b) N_e has reached an equilibrium value during the laser pulse. In addition, the recombination time $\tau_{rec}=1/[\alpha(T_e)N_e^2]$ is longer than the laser pulse length to ensure a slowly rising T_e as dictated by experimental results. Hence,

$$\frac{N_e}{N_{Na}-N_e}\propto\frac{1}{(N_{Na}-N_e)^{2/3}} \tag{8}$$

by setting Eq. (7) = 0.

Thus, a measure of the fractional ionization $N_e/(N_{Na}-N_e)$ obtained at the end of the laser pulse for different initial sodium densities N_{Na} should distinguish between cases (a) and (b). A plot of $N_e/(N_{Na}-N_e)$ versus $N_{Na}-N_e$ is shown in Fig. 9. The dashed line represents Eq. (8) normalized to the experimental point at $N_{Na}-N_e=10^{16}$ cm^{-3}. The good fit between theory and experiment signifies that the electron density yield was limited by collisional recombination.

The temporal history of N_e after the end of the laser pulse yields a lower bound for the three-body recombination time τ_{rec} of 100 ns for $N_e=2\times10^{16}$ cm^{-3}, $T_e=0.25$ eV. Hence $\alpha(0.25\text{ eV})$ is less than 3×10^{-26} cm^6 s^{-1} for sodium. Calculations for a model alkali-metal atom give a significantly higher recombination coefficient, $\alpha(0.25\text{ eV})=10^{-24}$ cm^6 s^{-1}.[24] The discrepancy is attributed to the inappropriate use of a hydrogenic-level scheme in these calculations.[25] The total recombination rate is well approximated by the collisional recombination rate into the highest levels n satisfying the condition that their electron excitation rates are less than their deexcitation rates.[26] In sodium, the critical levels n determined from inelastic collisional rates[11] for $T_e=0.25$ eV are the $4s$, $4p$, and $3d$ states, yielding $\alpha\approx3\times10^{-27}$ cm^6 s^{-1} which is consistent with experimental results.

D. Plasma lifetime

After reviewing all atomic and molecular processes, electron-ion thermalization was determined to be the predominant energy-loss mechanism for the free electrons. For $N_e=2\times10^{16}$ cm^{-3}, $T_e=0.25$ eV, $T_{oven}=0.07$ eV, and a thermalization time $\tau_{ei}=25$ ns,[23] the energy-loss rate is 4×10^4 W cm^{-3}. By comparison radiative losses in such low-temperature plasmas could only account for a maximum of 100 W cm^{-3}. Since the energy stored in the plasma was ≈0.02 J cm^{-3}, the minimum plasma lifetime

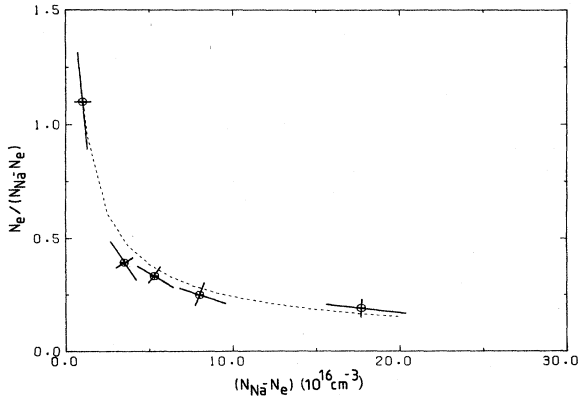

FIG. 9. Fractional ionization at the end of the laser pulse vs neutral density. Dashed line is a theoretical fit given by $N_e/(N_{Na}-N_e)\propto1/(N_{Na}-N_e)^{2/3}$.

should be 500 ns. In fact, the lifetime based on energy considerations should be longer than 500 ns since losses by thermalization terminate after a time $\tau_{ei}[(N_{Na^+}+N_{Na})/N_{Na^+}]=250$–300 ns, where thermalization of atoms during their ionized lifetime has been included by the factor $(N_{Na^+}+N_{Na})/N_{Na^+}$. The shorter decay times observed (200 ns in Fig. 4) suggest that diffusion governed the density decay.[8]

VI. SUMMARY

Resonant multiphoton ionization of sodium vapor yielded cold, dense plasmas similar to those described in I. Good agreement was found for the electron density determined from widths, shifts, and forbidden-component intensities. The minimum number of electrons per Debye sphere attainable in laser-pumped sodium vapor at densities 10^{16}–10^{18} cm^{-3} appears to be limited to approximately 1 by three-body recombination.

ACKNOWLEDGMENTS

We thank P. Ruthven for technical assistance on the oven and Professor D. D. Burgess, Dr. J. D. Kilkenny, and Dr. R. W. Lee for useful discussions. This work was supported by a Science and Engineering Research Council (SERC) grant.

---

*Present address: Lawrence Livermore National Laboratory, Livermore, CA 94550.

†Present address: British Aerospace, Bristol, England.

[1]P. Zoller and P. Lambropoulos, J. Phys. B **13**, 69 (1980).

[2]H. B. Bebb, Phys. Rev. **149**, 30 (1966).

[3]H. B. Bebb, Phys. Rev. **153**, 26 (1967).

[4]S. Geltman, J. Phys. B **13**, 115 (1980).

[5]N. L. Manakov, V. D. Ovsiannikov, M. A. Preobragenski, and L. P. Rapoport, J. Phys. B **11**, 245 (1978).

[6]P. Agostini, A. T. Georges, S. E. Wheatley, P. Lambropoulos, and M. D. Levenson, J. Phys. B **11**, 1733 (1978).

[7]S. J. Smith and P. B. Hogan, in *Laser Spectroscopy IV* (Springer, New York, 1979), p. 360.

[8]O. L. Landen, R. J. Winfield, D. D. Burgess, J. D. Kilkenny, and R. W. Lee, preceding paper, Phys. Rev. A **32**, 2963 (1985).

[9]C. A. van Dijk, P. J. Th. Zeegers, G. Nienhuis, and C. Th. J. Alkemade, J. Quant. Spectrosc. Radiat. Transfer **20**, 55 (1978).

[10]N. Aymar, E. Luc-Koenig, and F. Combet-Farnoux, J. Phys. B **9**, 2179 (1976).

[11]R. Shuker, A. Gallagher, and A. V. Phelps, J. Appl. Phys. **51**, 1316 (1980).

[12]E. M. Anderson and V. A. Zilitis, Opt. Spektrosk. **16**, 177 (1964) [Opt. Spectrosc. **16**, 99 (1964)].

[13]W. L. Wiese, M. W. Smith, and B. M. Miles, *Atomic Transition Probabilities* (U.S. National Bureau of Standards, Washington, D.C., 1969).

[14]J. Huennekens and A. Gallagher, Phys. Rev. A **27**, 1851 (1983).

[15]H. R. Griem, *Spectral Line Broadening in Plasmas* (Academic, New York, 1974).

[16]J. D. Kilkenny, R. W. Lee, M. H. Key, and J. G. Lunney, Phys. Rev. A **22**, 2746 (1980).

[17]J. J. de Groot and J. van Rooijen, in *Proceedings of the Twelfth International Conference on Phenomena in Ionized Gases (Eindhoven, 1975)*, edited by J. G. A. Hölscher and D. C. Schram (North-Holland, Amsterdam, 1975), p. 135.

[18]J. C. Stewart and K. D. Pyatt, Jr., Astrophys. J. **144**, 1203 (1966).

[19]K. W. Billman and J. R. Stallcop, Appl. Phys. Lett. **28**, 704 (1976).

[20]J. R. Stallcop and K. W. Billman, Plasma Phys. **16**, 1187 (1974).

[21]G. Peach, Mem. R. Astron. Soc. **71**, 1 (1967).

[22]M. Nishida, J. Phys. D **15**, 1951 (1982).

[23]L. Spitzer, Jr. and R. Härm, Phys. Rev. **89**, 977 (1952).

[24]D. R. Bates, A. E. Kingston, and R. W. P. McWhirter, Proc. R. Soc. London **267**, 297 (1962)

[25]J. Stevefelt, J. Boulmer, and J. F. Delpech, Phys. Rev. **12**, 1246 (1975).

[26]E. Hinnov and J. G. Hirschberg, Phys. Rev. **125**, 795 (1962).